Journal of Magnetism and Magnetic Materials 398 (2016) 32–37

Contents lists available at ScienceDirect

Journal of Magnetism and Magnetic Materials

journal homepage: www.elsevier.com/locate/jmmm

Transformation of hexagonal to mixed spinel crystal structure and magnetic properties of Co^{2+} substituted $BaFe_{12}O_{19}$

Varsha C. Chavan [a], Sagar E. Shirsath [b], Maheshkumar L. Mane [c,*], R.H. Kadam [d], Surendra S. More [a]

[a] Department of Physics, Yashawantrao Chavan Mahavidyalaya, Tuljapur, MS, India
[b] Department of Physics, Vivekanand College, Aurangabad 431001, MS, India
[c] Department of Physics, S. G. R. G. Shinde Mahavidyalaya, Paranda 413502, MS, India
[d] Materials Research Laboratory, Shrikrishna Mahavidyalaya, Gunjoti 413613, MS, India

ARTICLE INFO

Article history:
Received 24 May 2015
Received in revised form
11 July 2015
Accepted 1 September 2015
Available online 3 September 2015

Keywords:
M-type hexaferrites
XRD
FE-SEM
Magnetization

ABSTRACT

M-type barium hexaferrites $Ba_{1-x}Co_xFe_{12}O_{19}$ ($x=0.0$–1.00 with steps of 0.25) were synthesized by sol–gel autocombination method and were post-annealed at relatively low temperature at 600 °C. The samples were characterized by X-ray diffraction, scanning electron microscopy, infrared spectroscopy and vibrating sample magnetometry. Crystal transformed from pure Ba-hexaferrite to spinel with Co^{2+} substitution. Results of scanning electron microscope show that the grains are regular and well-defined structured. Infrared spectra support the nature and crystal symmetry that obtained from X-ray diffraction pattern study. Magnetization results show that saturation magnetization and magneton number decreased whereas coercivity increased for $x > 0.50$ Co^{2+} doping.

1. Introduction

Hexaferrites continue to be very attractive materials for technological applications due to their unique electrical and magnetic properties. The M-type hexaferrites $BaFe_{12}O_{19}$ are important ferromagnetic oxides due to their high intrinsic coercivity, fairly large crystalline anisotropy, high electrical resistivity and low cost. These properties make them potential candidate for their use in permanent magnets, recording media and microwave devices. Recently IBM has reported a magnetic tape composed of barium hexaferrite nanoparticles possessing 15 times higher recording density than the commercially available tapes in market. Barium hexaferrite is one of the most important commercial hard magnetic materials, representing the class of hexagonal M-type ferrites [1–5].

A variety of different cation substitutions are possible in $BaFe_{12}O_{19}$. Divalent transition metals such as $Ni^{2+}/^{3+}$ and $Co^{2+}/^{3+}$ for $Fe^{2+}/^{3+}$ are frequently used due to their similarity in ionic radii and electronic configurations. However, both the electrical and magnetic properties of substituted BaM ferrites are strongly dependent on the synthesis conditions as disproportionate charge distributions generally occur for multivalent cationic doping. There is also a concomitant structural implication when doping with $Co^{2+}/^{3+}$ ions influencing the magneto-dielectric properties of this compound. Thus, cobalt doping in particular has been the subject of many such investigations [6–8]. In this study the effect of Co^{2+} substitution in place of Ba^{2+} prepared by sol–gel auto-combustion technique has been discussed in details.

2. Experimental techniques

Stoichiometric Co^{2+} substituted $Ba_{1-x}Co_xFe_{12}O_{19}$ ($x=0.0$–1.00 with steps of 0.25) ferrite nanoparticles were prepared by the sol–gel auto-combustion technique using AR grade nitrates of respective cations $Ba(NO_3)_2 \cdot 6H_2O$, $Co(NO_3)_2 \cdot 6H_2O$, $Fe(NO_3)_3 \cdot 9H_2O$. Citric acid was used as chelating agent. All starting materials were dissolved in de-ionized water with required molarities. The metal nitrate to citric acid ratio was mentioned at 1:3. The solutions of the precursors were mixed and heated on hot plate with violent stirring. The pH of the solution plays a major role in the formation of a compound. The pH of the solution was kept at 8 by using ammonia solution. This final solution was consciously stirred to get fine particle size with greater homogeneity. The schematic presentation of prepared nanoparticles was shown in Fig. 1. The obtained fine particles were sintered at 600 °C for 6 h and used as

* Corresponding author.
E-mail address: mane.maheshkumar@hotmail.com (M.L. Mane).

http://dx.doi.org/10.1016/j.jmmm.2015.09.002
0304-8853/

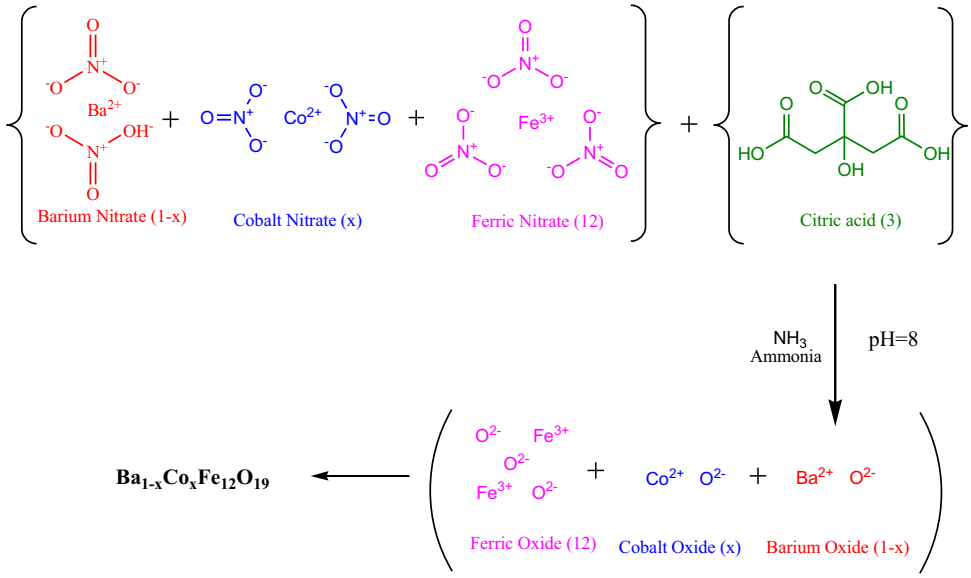

Fig. 1. Schematic presentation of $Ba_{1-x}Co_xFe_{12}O_{19}$ ($x=0.0$–1.00).

precursor for further characterizations.

X-ray diffraction patterns (XRD) were obtained using a Philips X-ray diffractometer (Model PW 3710) with Cu-K_α radiations ($\lambda=1.5405$ Å). The morphological investigations were carried out by using scanning electron microscopy techniques (SEM). The infrared (IR) spectra were recorded using Perkin-Elmer spectrometer. Vibrating sample magnetometer (VSM) was employed to characterize the magnetic properties.

3. Results and discussion

3.1. X-ray diffraction technique

The standard power X-ray diffraction technique in the region of $2\theta=20$–80 with a step scan of 0.02^o/min on a Philips diffractometer (Model PW1710) using CuKα radiation ($\lambda=1.5406$ Å) is employed at room temperature to study the crystal orientation of all the prepared samples of $Ba_{1-x}Co_xFe_{12}O_{19}$ ($x=0.0$–1.00) ferrite nanoparticles. The X-ray diffraction pattern for all the samples is shown in Fig. 2.

For all the supposed samples crystal structure was confirmed, i.e. for pure $BaFe_{12}O_{19}$ sample crystal structure is single phase hexagonal ferrite, while for $x=0.25$–0.75 the crystal structure shows phases of hexagonal as well as spinel ferrite. However, a small trace of residual α-Fe_2O_3, has been observed for Co^{2+} substituted samples. Due to Co^{2+} substitution in crystallographic site the peak positions are shifted to the right side of $BaFe_{12}O_{19}$ sample (Fig. 3). The results of XRD show that the strength of the peaks of $CoFe_2O_4$ phase increases as the doped Co^{2+} ion substitution increased. The similar results were found in literature for Co substituted $BaFe_{12}O_{19}$ and $SrFe_{12}O_{19}$ samples [9,10].

The presence of Co cation in the hexagonal structure, results in a slight change of diffraction peak position due to the slight change in the lattice parameters of the compounds. X-ray diffraction pattern of these samples reveals that the reference peaks of hematite (Fe_2O_3) and Cobalt iron oxide ($CoFe_2O_4$ and $BaFe_{12}O_{19}$) are seen from JCPDS 85-0987, JCPDS 22-1086 and JCPDS 43-0002, respectively. However, for $x=1.00$ the sample shows the single phase cubic spinel structure with α-Fe_2O_3 as a secondary phase.

The physical properties of ferrite nanoparticles, such as the lattice constants of (a and c) and cell volume V of respective ferrites were calculated from the X-ray diffraction data and they are

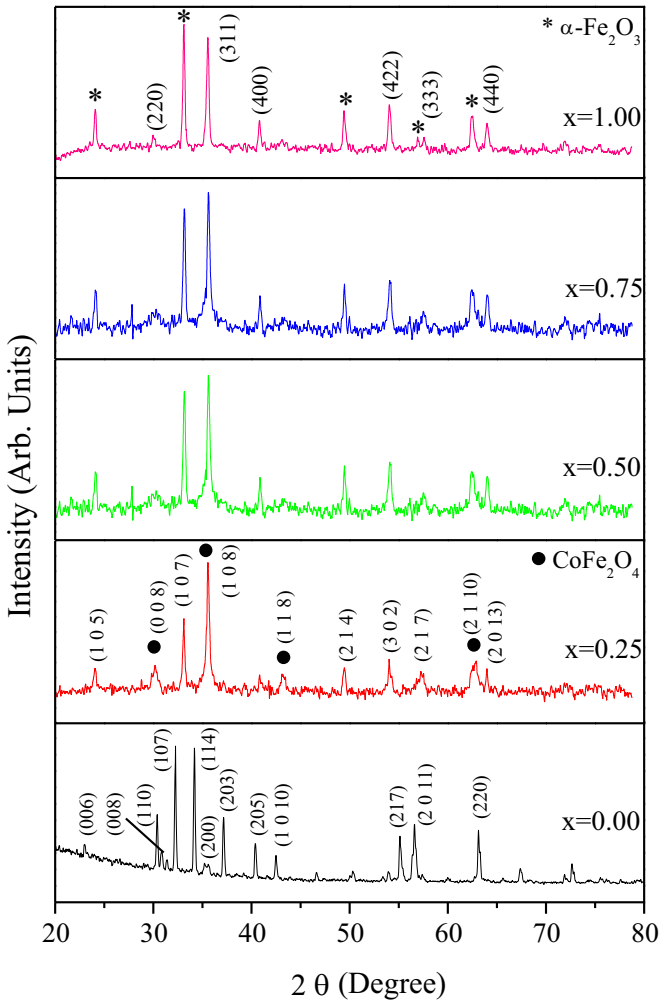

Fig. 2. X-ray diffraction pattern for $Ba_{1-x}Co_xFe_{12}O_{19}$ ($x=0.0$–1.00).

tabulated in Table 1. The data reported in Table 1 indicates that both lattice constants (a and c) and cell volume V decreases as Co^{2+} cation concentration increases upto $x=0.75$. An oblivious decrease in the lattice constant can be related to the replacement

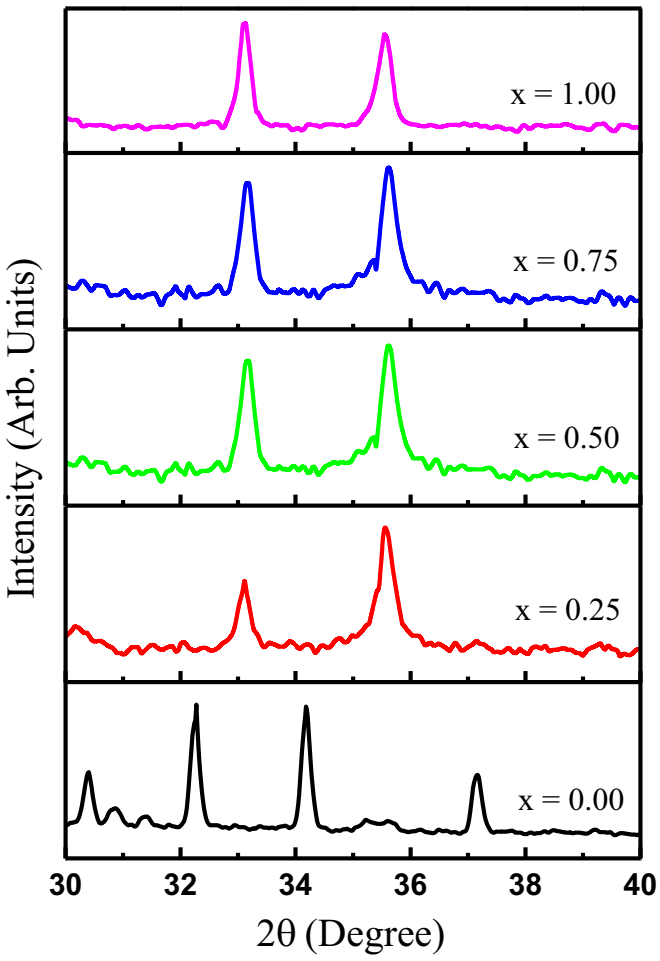

Fig. 3. Maximum of X-ray diffraction pattern for $Ba_{1-x}Co_xFe_{12}O_{19}$ (x=0.0–1.00).

Table 1
Values of Lattice constant '*a*' and '*c*', *c*/*a* ration, cell volume '*V*', particle size '*D*', for $Ba_{1-x}Co_xFe_{12}O_{19}$.

X	*a* (Å)	*c* (Å)	*c*/*a*	*V* (Å)^3	*D* (nm)
0.0	5.889	23.67	4.019	710.906	34.45
0.25	5.869	23.45	3.995	699.523	35.18
0.50	5.822	23.14	3.974	679.264	39.04
0.75	5.813	22.79	3.920	666.923	47.38
1.00	8.326	–	–	–	49.69

of larger ionic radii Ba^{2+} (1.42 Å) by smaller ionic radii of Co^{2+} (0.74 Å) cation.

The crystallite size '*D*' can be measured by the Scherrer equation which is expressed as

$$D = \frac{0.9\,\lambda}{\beta \cos\theta} \quad (1)$$

where 'λ' is wave length, 'β' is FWHM and 'θ' is the Bragg angle. The values of measured crystalline size are reported in Table 1. The crystallite size is found to be in the range of 34.45–49.69 nm.

X-ray density (theoretical density) 'd_x' is calculated by the formula

$$d_x = \frac{2\,M}{N_A\,V} \quad (2)$$

where numeric factor denotes the number of formula units in a unit cell, '*M*' is the molar mass, 'N_A' is the Avogadro's number and

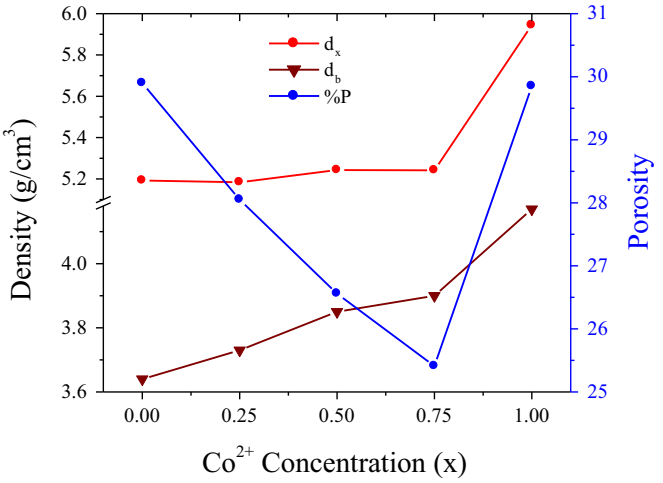

Fig. 4. Variation of X-ray density, bulk density and porosity of $Ba_{1-x}Co_xFe_{12}O_{19}$ (x=0.0–1.00).

'*V*' is the unit cell volume. The bulk density (d_b) and porosity (*%P*) was also calculated [11] and porosity with Co^{2+} ion content is shown in Fig. 4 and it is observed that X-ray density initially decreases for x=0.25 and then increases as the Co^{2+} ion concentration increases. The X-ray density is higher than the bulk density which might be due to the presence of pores occurred during the sintering process.

3.2. Scanning electron microscopy

To analyze the particle sizes and particle size distributions of the synthesized nanopowders, their Scanning Electron Microscopy (SEM) (JEOL-JSM 6360A) images for different concentrations of Co^{2+} ions in $Ba_{1-x}Co_xFe_{12}O_{19}$ (x=0.0, 0.50 and 1.00) were carried out and these images are presented in Fig. 5. As can be seen from this figure, the distribution of particle size is almost homogeneous and the average particle sizes are below 100 nm for all of the samples, but the particles are agglomerated. The agglomeration of nanoparticles may be attributed to the magnetic interactions between them.

3.3. Fourier infrared spectroscopy

Fourier infrared spectra of all the samples of the $Ba_{1-x}Co_xFe_{12}O_{19}$ (x=0.0–1.00) ferrite nanoparticles were recorded at room temperature in the range 400–4000 cm^{-1} on a Perkin Elemer spectrometer (Model 783). To study the FTIR spectra of all the samples, about one gram of fine powder of each sample was mixed with KBr in the ratio 1:250 by weight to ensure uniform distribution in the KBr pellet. The mixed powder was then pressed in a cylindrical die to obtain clean disk of approximately 1 mm thickness. The IR spectra were used to locate the band position. The infrared spectra reviles the detailed information about the structural changes occurred due to the Co^{2+} substitution in $BaFe_{12}O_{19}$ M-type hexaferrite material. The positions of all adsorption bands of the products are very similar, while their relative intensities varied (Fig. 6).

The spectra recorded for all the samples shows two strong characteristic absorption bands in the area between 400 cm^{-1} and 800 cm^{-1}, which are related to the Fe–O stretching vibration band in octahedral and tetrahedral sites [12–14]. Band in the range 420–443 cm^{-1} corresponds to the assignment of Fe–O bending by Fe–O_4 and Fe–O stretching by Fe–O_6 whereas, the band in the range 530–550 cm^{-1} corresponds to the Fe–O stretching by Fe–O_4. The gradual shift of these bands towards low frequency side with

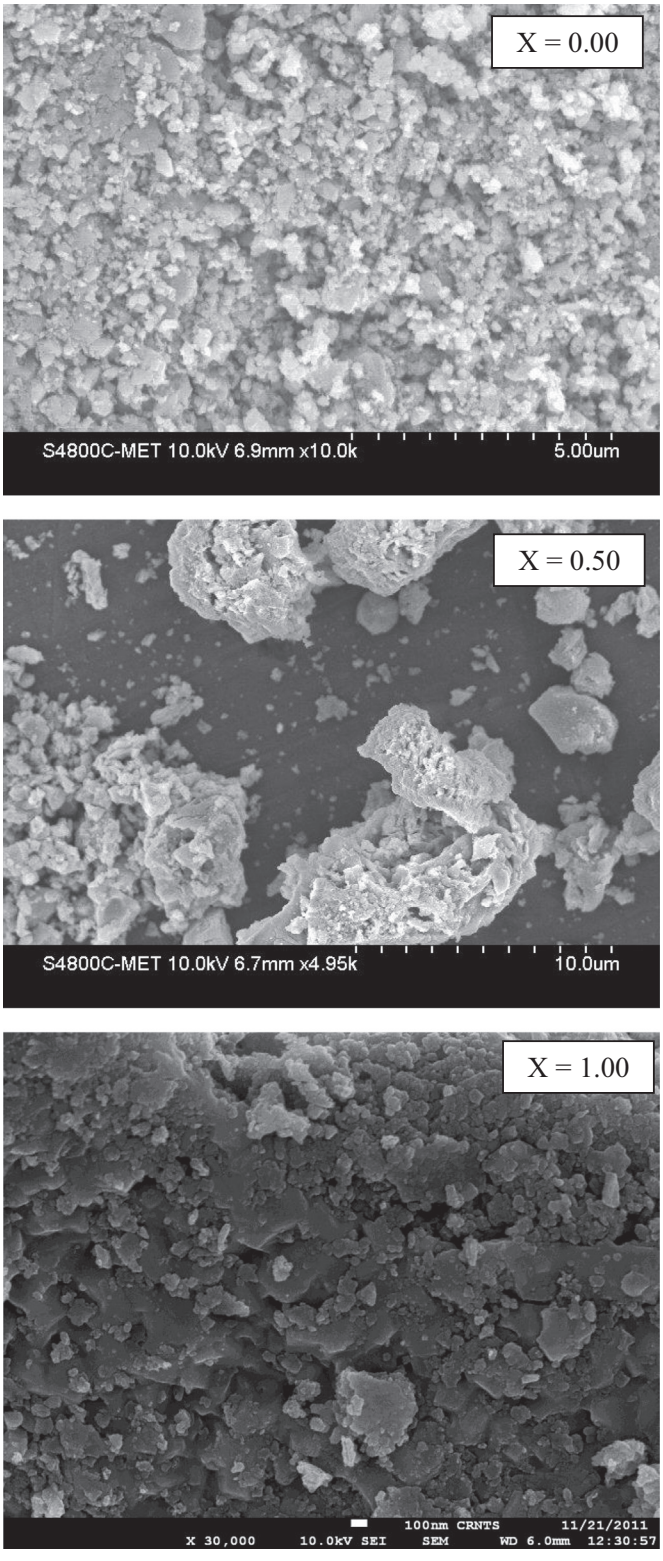

Fig. 5. Scanning electron microscopy images of $Ba_{1-x}Co_xFe_{12}O_{19}$ (x=0.00, 0.50 and 1.00).

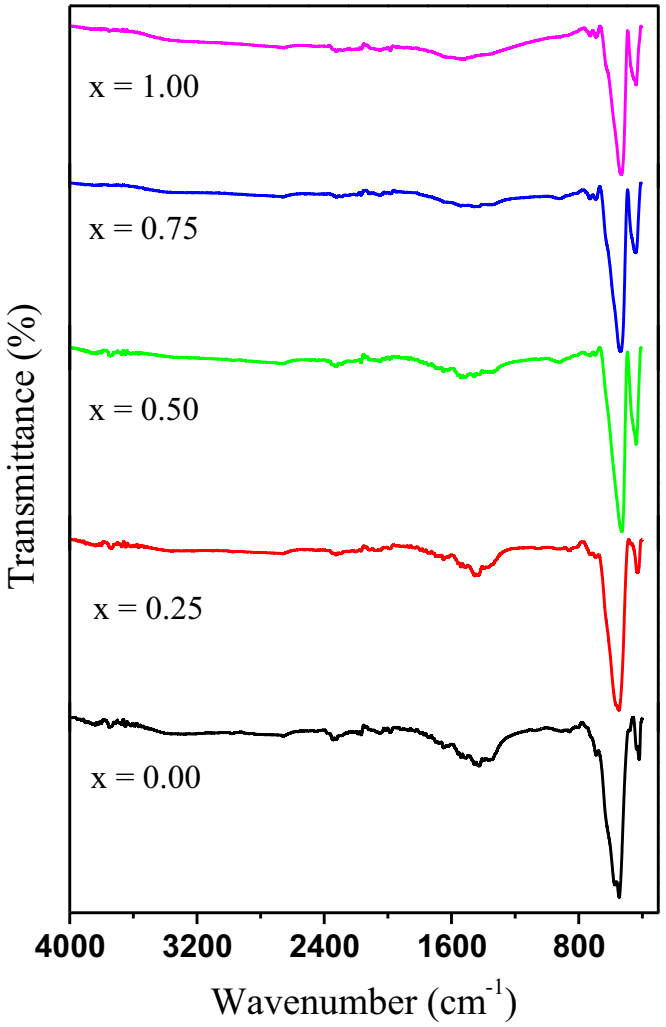

Fig. 6. Fourier infrared spectra of $Ba_{1-x}Co_xFe_{12}O_{19}$ (x=0.0–1.00).

increase in Co^{2+} contents can be attributed to the substitution of large Co^{2+} ions affecting the distribution of Fe^{3+} ions. For the undoped ferrite, the absorption peak at about 579 cm^{-1} is distinguished which is associated with Ba–O stretching vibration band (Fig. 7). This peak cannot be observed in the doped samples [15]. The small absorption peak (for x=0.00 and 0.25) in the range 1360–1460 cm^{-1} related to M–O–M bands (Metal–Oxygen–Metal) such as Co–O–Co and Fe–O–Fe bands [14,15].

3.4. Magnetization

The magnetic properties such as saturation magnetization (Ms) and coercivity (Hc) are calculated from the hysteresis loops (Fig. 8) for different values of x measured at room temperature and the results are listed in Fig. 9. The hysteresis loops for $Ba_{1-x}Co_xFe_{12}O_{19}$ (x=0.00, 0.25, 0.50, 0.75 and 1.00) ferrites are shown in Fig. 8.

Generally, the magnetic behavior of the hexaferrite is governed by the distribution of iron ions in the crystallographic lattice sites. It is known that there are five substitutional sites for iron in the hexagonal structure of barium hexaferrite which are denoted by 12k, 2a, 2b, $4f_1$ and $4f_2$. The sites of 12k, 2a and 2b have upward spin direction, while the $4f_1$ and $4f_2$ sites have downward spin directions [14]. It was reported that Co^{2+} ions occupy both the tetrahedral 4f1 and octahedral $4f_2$ positions [16,17] by assuming that cobalt ions hardly enter 2a positions. As a result of high Co substitution saturation magnetization is slightly less than that of the pure $BFe_{12}O_{19}$. The presence of α-Fe_2O_3, which is a canted antiferromagnet, may also contribute to the reduction in magnetization values.

The observed magneton number (n_B) was calculated from the measured saturation magnetization (σ_s) using the following formula [18] and the values are presented in Fig. 9:

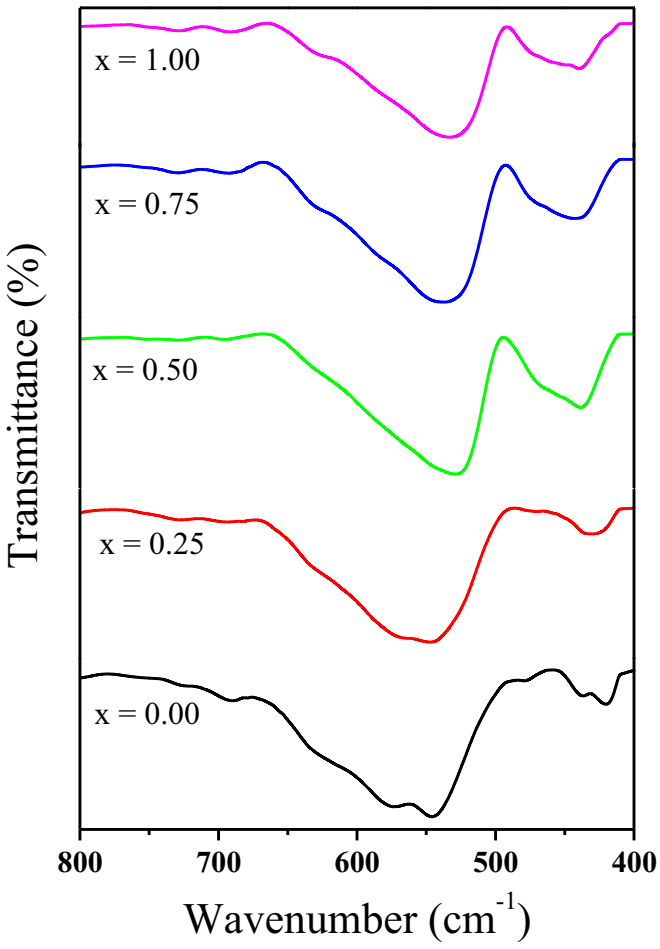

Fig. 7. Maximum of FTIR spectra of $Ba_{1-x}Co_xFe_{12}O_{19}$ (x=0.0–1.00).

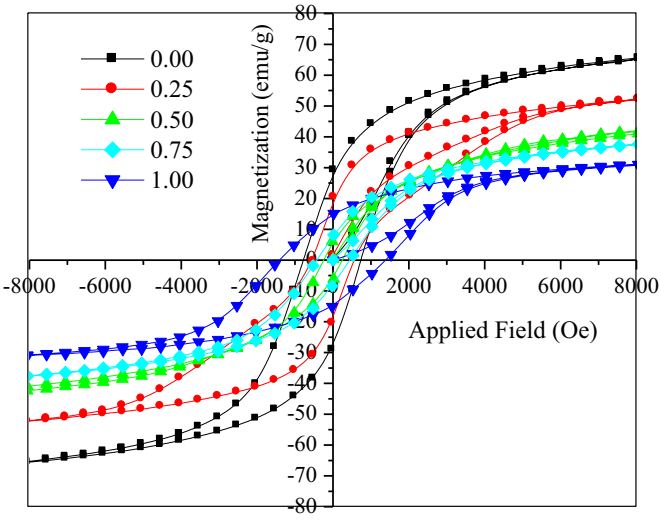

Fig. 8. Magnetic hysteresis loops of $Ba_{1-x}Co_xFe_{12}O_{19}$ (x=0.0–1.00).

$$n_B = \frac{\text{M. W.} \times \text{Ms}}{5585} \quad (3)$$

where M.W. is molecular weight of compound and Ms is saturation magnetization. It is observed from Fig. 9 that the values of observed magneton number (n_B) decreases as the Co^{2+} ion concentration increases. The decrease in Ms and n_B is attributed to the transformation of hexagonal to spinel structure. This may also relate to weakening in magnetic integrations among Co^{2+}, Ba and Fe^{3+} ions.

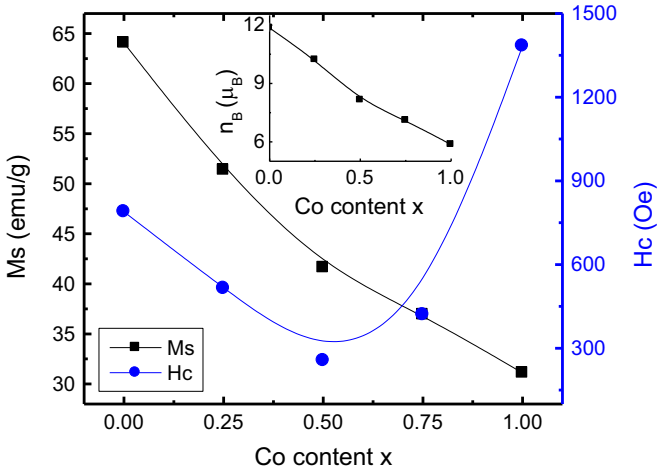

Fig. 9. Variation of saturation magnetization (Ms), Coercivity (Hc) and observed magneton number (n_B).

It is observed from Fig. 9 that coercivity initially decreased for x=0.5, latter on it shows increasing trend with increase in Co substitution. The decrease in Hc could be due to mixed phase of spinel and hexaferrite structure. Samples $x > 0.5$ shows increasing trend, this may be due to the dominance of spinel structure over hexaferrite structure. The increase in Hc for $x > 0.5$ may also be related to increase in magneto-crystalline anisotropy with Co substitution.

4. Conclusions

Series of barium hexaferrites substituted with divalent Co ions with chemical formulae $Ba_{1-x}Co_xFe_{12}O_{19}$ (x=0.0, 0.25, 0.50, 0.75 and 1.0) were successfully prepared by the sol–gel auto-combustion technique. X-ray diffraction investigation performed at room temperature shows formation of single phase hexagonal structure for undoped BaM and indicates influence of substitution on the structure of material. $BaFe_{12}O_{19}$ sample crystal structure is single phase hexagonal ferrite, while for x=0.25–1 the crystal structure shows phases of hexagonal as well as spinel ferrite. The different physical parameters such as lattice constants, X-ray density, cell volume, porosity, particle size were measured. The measured particle size of Co^{2+} substituted BaM is in the range of 34–50 nm. The knowledge of phase formation and surface morphology was understood by scanning electron microscopy technique. It is observed that Co^{2+} substitution greatly affects the grain size and morphology of barium hexaferrite. FTIR patterns support the XRD results and show the shifting in absorption bands. Magnitude of Ms and Hc are related to the distribution of dopant ions on the five sites in the crystallattice. Both the nature and concentration of dopants monitor site preferences. Increase in Hc is attributed to increase in magneto-crystalline anisotropy.

References

[1] R.C. Pullar, Hexagonal ferrites: a review of the synthesis, properties and applications of hexaferrite ceramics, Prog. Mater. Sci. 57 (2012) 1191–1334.
[2] R.S. Alam, M.K. Tehrani, M. Moradi, E. Hosseinpour, A. Sharbati, The role of matching thickness on the wideband electromagnetic wave suppresser using single layer doped barium ferrite, J. Magn. Magn. Mater. 323 (2011) 1040–1043.
[3] Z. Yang, C.S. Wang, X.H. Li, H.X. Zeng, (Zn, Ni, Ti) substituted barium ferrite particles with improved temperature coefficient of coercivity, Mater. Sci. Eng.:

B 90 (2002) 142–145.
[4] E.V. Pashkova, E.D. Solovyova, T.V. Kolodiazhnyi, V.P. Ivanitskii, A.G. Belous, Effect of heat treatment on the phase composition, structure and magnetic properties of M-type barium hexaferrite, J. Magn. Magn. Mater. 368 (2014) 1–7.
[5] A. Lisfi, J.C. Lodder, Relation between the microstructure and magnetic properties of $BaFe_{12}O_{19}$ thin films grown on various substrates, J. Magn. Magn. Mater. 242–245 (2002) 391–394.
[6] R. Carey, P.A. Gago-Sandval, D.M. Newman, B.W.J. Thomas, The magnetic and magneto-optical properties of Co, Cr, Mn and Ni substituted barium ferrite films, J. Appl. Phys. 75 (1991) 6789–6791.
[7] X. Batlle, X. Obradors, J. Rodríguez-Carvajal, M. Pernet, M.V. Cabañas, M. Vallet, Cation distribution and intrinsic magnetic properties of Co-Ti-doped M-type barium ferrite, J. Appl. Phys. 70 (1991) 1614.
[8] X. Batlle, M. García del Muro, J. Tejada, H. Pfeiffer, P. Görnert, E. Sinn, Magnetic study of M-type doped barium ferrite nanocrystalline powders, J. Appl. Phys. 74 (1993) 3333.
[9] Darja Lisjak, Giovanni Bolelli, Luca Lusvarghi, Marion Begard, Markus Bruehl, Kirsten Bobzin, Pertti Lintunen, Ulla Kanerva, Massimo Pasquale, Miha Drofenik, Magnetic phase formation in CoTi-substituted Ba hexaferrite coatings prepared with atmospheric plasma spraying, J. Am. Ceram. Soc. 93 (9) (2010) 2579–2584.
[10] S.E. Mousavi Ghahfarokhi, F. Ranjbar, M. Zargar Shoushtari, A study of the properties of $SrFe_{12-x}Co_xO_{19}$ nanoparticles, J. Magn. Magn. Mater. 349 (2014) 80–87.
[11] Vinod N. Dhage, M.L. Mane, M.K. Babrekar, C.M. Kale, K.M. Jadhav, Influence of chromium substitution on structural and magnetic properties of $BaFe_{12}O_{19}$ powder prepared by sol–gel auto combustion method, J. Alloy. Compd. 509 (2011) 4394–4398.
[12] G.R. Gordani, A. Ghasemi, A. Saidi, Enhanced magnetic properties of substituted Sr-hexaferrite nanoparticles synthesized by co-precipitation method, Ceram. Int. 40 (2014) 4945–4952.
[13] A. Baniasadi, A. Ghasemi, A. Nemati, M.A. Ghadikolaei, E. Paimozd, Effect of Ti–Zn substitution on structural, magnetic and microwave absorption characteristics of strontium hexaferrite, J. Alloy. Compd. 583 (2014) 325–328.
[14] S.K. Chawla, R.K. Mudsainiyan, S.S. Meena, S.M. Yusuf, Sol–gel synthesis, structural and magnetic properties of nanoscale M-type barium hexaferrites $BaCo_xZr_xFe_{(12-2x)}O_{19}$, J. Magn. Magn. Mater. 350 (2014) 23–29.
[15] Reza Shams Alam, Mahmood Moradi, Mohammad Rostami, Hossein Nikmanesh, Razieh Moayedi, Yang Bai, Structural, magnetic and microwave absorption properties of doped Ba-hexaferrite nanoparticles synthesized by co-precipitation method, J. Magn. Magn. Mater. 381 (2015) 1–9.
[16] Z. Simsa, S. Logo, R. Gerber, E. Pollert, Cation distribution in Co-Ti-substituted barium hexaferrites: a consistent model, J. Magn. Magn. Mater. 140–144 (1995) 2103–2104.
[17] J.M. Williams, J. Adetunji, M. Gregori, Mössbauer spectroscopic determination of magnetic moments of Fe^{3+} and Co^{2+} in substituted barium hexaferrite, $Ba_{(Co,Ti)x}Fe_{(12-2x)}O_{19}$, J. Magn. Magn. Mater. 220 (2000) 124–128.
[18] Maheshkumar L. Mane, R. Sundar, K. Ranganathan, S.M. Oak, K.M. Jadhav, Effects of Nd:YAG laser irradiation on structural and magnetic properties of $Li_{0.5}Fe_{2.5}O_4$, Nucl. Instrum. Methods Phys. Res. Sect. B: Beam Interact. Mater. At. 269 (2011) 466–471.